Production of high-resolution reference polarization images from real world scenes

Bigué Laurent, Alban Foulonneau, Pierre-Jean Lapray

PROCEEDINGS OF SPIE

SPIEDigitalLibrary.org/conference-proceedings-of-spie

Production of high-resolution reference polarization images from real world scenes

Laurent Bigué, Alban Foulonneau, Pierre-Jean Lapray

Laurent Bigué, Alban Foulonneau, Pierre-Jean Lapray, "Production of high-resolution reference polarization images from real world scenes," Proc. SPIE 12690, Polarization Science and Remote Sensing XI, 126900B (3 October 2023); doi: 10.1117/12.2677421

SPIE.

Event: SPIE Optical Engineering + Applications, 2023, San Diego, California, United States

Production of high-resolution reference polarization images from real world scenes

Laurent Bigué[a,b], Alban Foulonneau[a,b], and Pierre-Jean Lapray[a,b]

[a]Université de Haute-Alsace, IRIMAS UR 7499, F-68100 Mulhouse, France
[b]Université de Strasbourg, France

ABSTRACT

A few polarization image datasets depicting real world scenes have been reported. Some of them are available on an open-data basis. Some databases contain color images, often with color bands reconstructed from a sensor equipped with a Bayer filter. Unfortunately, even if these real-world images depict a variety of objects and situations and have a good overall quality (ie the spectral bands and the various polarization channels are or can be registered, noise is reduced), they often have a low definition (smaller than 1 Mp), a low bit depth and are captured with a large lens aperture, resulting in very band-limited images. Moreover, the demosaicing procedure used to reconstruct the various color bands has a smoothing effect, reducing their resolution. This latter point proves detrimental when it comes to use these images as references for demosaicing algorithms, especially for RGB images: since each channel combining polarization direction and spectral band is very sparse in the base mosaic pattern, artifacts likely to appear are considerably underestimated with band-limited images. In this work, we review existing polarization image databases, focus on non-mosaiced datasets and propose a technique to produce HD polarization images with superior quality.

Keywords: Polarization imaging, database, mosaicing, registration

1. INTRODUCTION

Some polarization image databases or datasets depicting real world scenes have been reported over the past few years.[1–18] Availability of high bandwidth communication networks and large data repositories allows researchers to easily share reference databases, especially with the development of open data. Their content is diverse, as well as the way they were captured. Some of them are rather dedicated to testing new vision algorithms, whereas others were made for general purpose, including low-level demosaicing algorithms required by sensors equipped with microgrid polarimeters arrays (sometimes named Polarizer Filter Arrays or PFAs).

All of these datasets include polarization information, either images in various polarization directions or Stokes information. Most of them contain color information, and some of them, dedicated to vision applications, also contain depth information grabbed with an additional sensor. All of them claim they contain ground truth data. Nevertheless, images produced from mosaic array sensors, either with polarization microgrids or a color array, should not be considered as ground truth references when used for testing low level algorithms such as demosaicing algorithms.

In this work, we will review and benchmark existing databases and then will propose to make HD polarimetric images free from common defects, especially misregistration between polarization and color bands.

In Section 2, polarization basics will be briefly recalled. In Section 3, polarization databases and datasets will be reviewed and we will focus on the databases containing full definition data (ie non interpolated from a microarray sensor). In Section 4 we will describe metrics well suited to polarization images. Then Section 5 will propose and implement several recommendations for making HD polarization images.

Further author information: (Send correspondence to L.B.)
L.B.: E-mail: laurent.bigue@uha.fr

Polarization Science and Remote Sensing XI, edited by Meredith K. Kupinski, Joseph A. Shaw, Frans Snik, Proc. of SPIE Vol. 12690, 126900B
 · 0277-786X · doi: 10.1117/12.2677421

2. POLARIZATION BASICS

In the following, we will only deal with linear polarization, but such considerations can easily be extended to elliptical polarization which is the most general case. Capturing polarization in an imaging way consists in grabbing images with a polarization state analyzer (PSA). In the case of linear polarization, the polarization state analyzer is often a camera equipped with a linear polarizer the orientation of which can be precisely controlled.[19] In order to speed up the process, the rotating polarizer can be replaced with a fixed polarizer and a liquid crystal cell.[20] Another very popular solution is to use a camera equipped with an array of micropolarizers,[21] but it requires a demosaicing procedure which can create more or less noticeable artifacts.[22]

At least N=3 different orientations of the polarizer are required to estimate the full linear polarization information. Using $N > 3$ orientations allows to reduce noise. It can be shown that using equally spread angles over [0;180°] optimizes the precision of the estimation process.[21] Therefore, it is quite a common strategy to capture polarization information with a polarizer oriented at $\{0,\ 45,\ 90,\ 135\}^\circ$. We name the corresponding intensities I_0, I_{45}, I_{90} and I_{135}. From these raw images, we first estimate Stokes parameters related to linear polarization

$$s_0 = \frac{1}{2}(I_0 + I_{45} + I_{90} + I_{135}), \qquad s_1 = I_0 - I_{90}, \qquad s_2 = I_{45} - I_{135}, \tag{1}$$

and then common polarization metrics, namely degree of linear polarization ($DoLP$) and angle of polarization ($AoLP$)

$$DoLP = \frac{\sqrt{s_1^2 + s_2^2}}{s_0}, \qquad AoLP = \frac{1}{2}\arctan\left(\frac{s_2}{s_1}\right). \tag{2}$$

3. OVERVIEW OF EXISTING POLARIZATION DATABASES

3.1 Overview of existing polarization databases

Some polarization image databases or datasets depicting polarization scenes have been reported in the literature over the last few years.[1–18] They contain the capture of various scenes under natural or artificial (be it controlled or not) illumination. They present very different characteristics: some of them are partly synthetic, some of them also contain depth information, ... They were used for testing algorithms, ranging from demosaicing algorithms to segmentation algorithms. Tab. 1 summarizes basic characteristics of these various datasets. This table, regularly updated, is available online.[23] It contains information found in the referenced papers as well as that provided by their authors in response to our questions.

In the following, we will focus on the full definition datasets -we will name them non-interpolated datasets-, not produced with polarization or color filter array sensors, that can be used for testing demosaicing algorithms.

3.2 Polarization datasets usable for testing demosaicing algorithms

We will now only consider the 5 full definition polarization databases with more than 20 scenes,[3,5–7,10] produced by sensors not using any micro-filters, since they are the only ones to contain non interpolated ground-truth data. Therefore, they can be used for testing demosaicing algorithms without any bias due to previous interpolation.

Tab. 2 reports information about the images. Among the 5 considered databases, Sargent's sounds very interesting since it provides the images with the largest definition and the largest bit-depth. Moreover, the limited lens aperture has probably produced sharp images.

In the following we will focus on the objective quality of the images. A further step would be to get interested in the polarimetric content of the images, as Sargent *et al.*[6] did.

4. EVALUATION CRITERIA

In the following, we focused on two characteristics of images in the various datasets: alignment of the various color and polarization channels, likely to create polarization artifacts, and image sharpness, since demosaicing artifacts may appear more easily in sharp images.

Table 1: Basic characteristics of imaging polarization datasets. Empty cells means that no information was available. An up-to-date version of the table is available online.[23]

dataset	availability	number of scenes	definition	bit-depth	mosaiced sensor	mono / color
Abubakar[1]		6	1280 x 960	8	NO	mono
Lapray[2]	GitHub	10	1024 x 768	12	yes	RGB/IR
Qiu[4]	univ. repository	40	1024 x 1024	8	yes	RGB
Zeng ('Forknet')[3]	upon request	120	1280 x 960	8	NO	mono
Wen 2019[5]	GitHub	105	1456 x 1088	8	NO	RGB
Morimatsu[7]	univ. repository	40	1024 x 768	10	NO	RGB
Sargent[6]		24	2448 x 2048	10 or 12	NO	mono
Ba[9]	google drive	326	1024 x 1024	11	yes	RGB
Wen 2021a[10]	GitHub	40+10	720 x 540	8	NO	RGB
Wen 2021b[11]	GitHub	8	1384 x 1032	8	yes	RGB
Blin[12]	zenodo.org	2060	500 x 500	8	yes	RGB
Sun[13]	google drive	132	2048 x 1848	8	yes	RGB
Sattar[14]	GitHub	28	1224 x 1024	8	yes	RGB
Lei[15]	GitHub	522	1224 x 1024	11	yes	RGB
Ono[16]	upon request	82	2448 x 2040	11	yes	RGB
Kurita[17]	upon request	729+82+238	2448 x 2048	12	yes	RGB
Liu[18]	upon request	200+100	2448 x 2048		yes	RGB

4.1 Shift between polarization channels

First, we report imaging metrics for a scene ('bottle') extracted from Morimatsu *et al.*'s[7] dataset in Fig. 1. *DoLP* and *AoLP* are evaluated in the green band. As for many images in this dataset or in other datasets, much information appears in *DoLP* images (Fig. 1(b) and (e)), at the edges of objects or on textured objects. But this information looks like an edge extraction: the original polarization images in the four directions are shifted and produce polarization artifacts. This phenomenon is well known[24] and should be compensated for: even a $1/20^{\text{th}}$ pixel shift causes noticeable polarization metrics degradation. We only considered shift caused by translation and we evaluated the subpixel shifts with an automated algorithm based on correlation[25] over the considered datasets. We found that mean shifts between each polarization direction could be as high as 1 pixel. Shifts between color bands are also noticeable. We register the green and blue bands onto the red band and the original polarization images I_{45}, I_{90} and I_{135} onto I_0 with a uniform rigid translation.[25] We report the result of this operation for the 'bottle' scene from Morimatsu's dataset in Fig. 1 (g)-(l). The changes in s_0 images are not spectacular. It is different for polarization images: most artifacts disappear, and we obtain what is probably close to genuine polarization information.

We detail in Tab. 3 the average shifts between polarization images for Morimatsu's database (but other databases are also concerned). For each considered database, we report in Tab. 4 average and maximum figures of shift between all polarization directions.

For instance, Wen *et al.*'s 2019 database presents a low shift between original polarization images and registering them does not provide any significant improvement. Shift figures for 'Forknet' database are high, but the authors clearly mention the phenomenon in their paper and the solution (ie the rigid registration) to alleviate it. Such a shift is therefore a problem only if you do not compensate for it.

4.2 Image sharpness

It seems reasonable that the evaluation of demosaicing algorithms in a precise way requires sharp images. Many metrics can be used to evaluate blur;[26] we chose to use no-reference bounded blur metrics[27,28] to evaluate image sharpness. They give similar results for the datasets we tested, we will only report in the following Cumulative Probability of Blur Detection (CPBD) figures.[28]

Table 2: Characteristics of datasets with full-definition images. An up-to-date version of the table is available online.[23]

dataset	**Forknet**[3]	**Wen 2019**[5]	**Sargent**[6]	**Morimatsu**[7]	**Wen 2021a**[10]
number of scenes	120	105	24	40	50
definition	1280 x 960	1456 x 1088	2448 x 2048	1024 x 768	720 x 540
spectral bands	mono	RGB	mono	RGB	RGB
bit-depth	8	8	10 or 12	10	8
camera	Point Grey BFLY-U3-23S6M-C	JAI AP-1600T-USB	Blackfly	JAI CV-M9GE 3-CCD	FLIR BFS-U3-04S2m-cs
sensor	Sony IMX249	3x Sony IMX273	Sony IMX250	Sony ICX204AL	Sony IMX287
sensor technology	CMOS	CMOS	CMOS	CCD	CMOS
pixel pitch (µm)	5.86	3.45	3.45	4.65	6.9
averaged images	1	1	50	1000	1
PSA type	rotating pol. + CMOS	rotating pol. + prism + 3 CMOS	rotating pol. + CMOS	prism + 3 CCD	rotating pol. + rotating color wheel + CMOS
polarizing element			Tiffin 49CP 49mm polarizer	Sigmakoki SPF-50C-32	
objective lens			Fujinon 12.5mm 2/3"		
lens aperture	fixed	f/1.4	f/8		f/1.4

Table 3: Shifts (in pixels) between polarization directions for Morimatsu *et al.*'s database (average figures over the whole dataset).

Red band				
	$\boldsymbol{I_0}$	$\boldsymbol{I_{45}}$	$\boldsymbol{I_{90}}$	$\boldsymbol{I_{135}}$
$\boldsymbol{I_0}$		0.34	0.20	0.35
$\boldsymbol{I_{45}}$	0.34		0.25	0.59
$\boldsymbol{I_{90}}$	0.20	0.25		0.35
$\boldsymbol{I_{135}}$	0.35	0.59	0.35	

Green band				
	$\boldsymbol{I_0}$	$\boldsymbol{I_{45}}$	$\boldsymbol{I_{90}}$	I_{135}
$\boldsymbol{I_0}$		0.34	0.20	0.34
$\boldsymbol{I_{45}}$	0.34		0.26	0.60
$\boldsymbol{I_{90}}$	0.20	0.26		0.35
$\boldsymbol{I_{135}}$	0.34	0.60	0.35	

Blue band				
	$\boldsymbol{I_0}$	$\boldsymbol{I_{45}}$	$\boldsymbol{I_{90}}$	$\boldsymbol{I_{135}}$
$\boldsymbol{I_0}$		0.33	0.21	0.32
$\boldsymbol{I_{45}}$	0.33		0.24	0.56
$\boldsymbol{I_{90}}$	0.21	0.24		0.33
$\boldsymbol{I_{135}}$	0.32	0.56	0.33	

Fig. 2 reports CPBD figures for all available non-mosaiced datasets. The datasets with sharper images are reported to be Wen *et al.*'s 2019 dataset and 'Forknet' dataset. We verified (Fig. 3) that blur figures were independent of image size and compared, for Wen's 2019 database, images at the original definition (1456x1088), cropped images (definition is 720x540, and the field of view is reduced) and resized images (definition is 720x540, and the field of view is that of original images). Cropped images exhibit CPBD figures somewhat similar to original images whereas resized images exhibit lower CPBD figures. Therefore, the CPBD metric seems only dependent on the image sharpness.

Nevertheless, blur figures must be considered with much caution. Fig. 4 displays the I_0 images in the various color bands of scene #44 from Wen *et al.*'s 2019 dataset as well as corresponding CPBD figures. CPBD figures are much higher for the blue band, whereas it appears blurry. We also tried the blur metric proposed by Crété *et al.*[27] which also produced counter-intuitive figures.

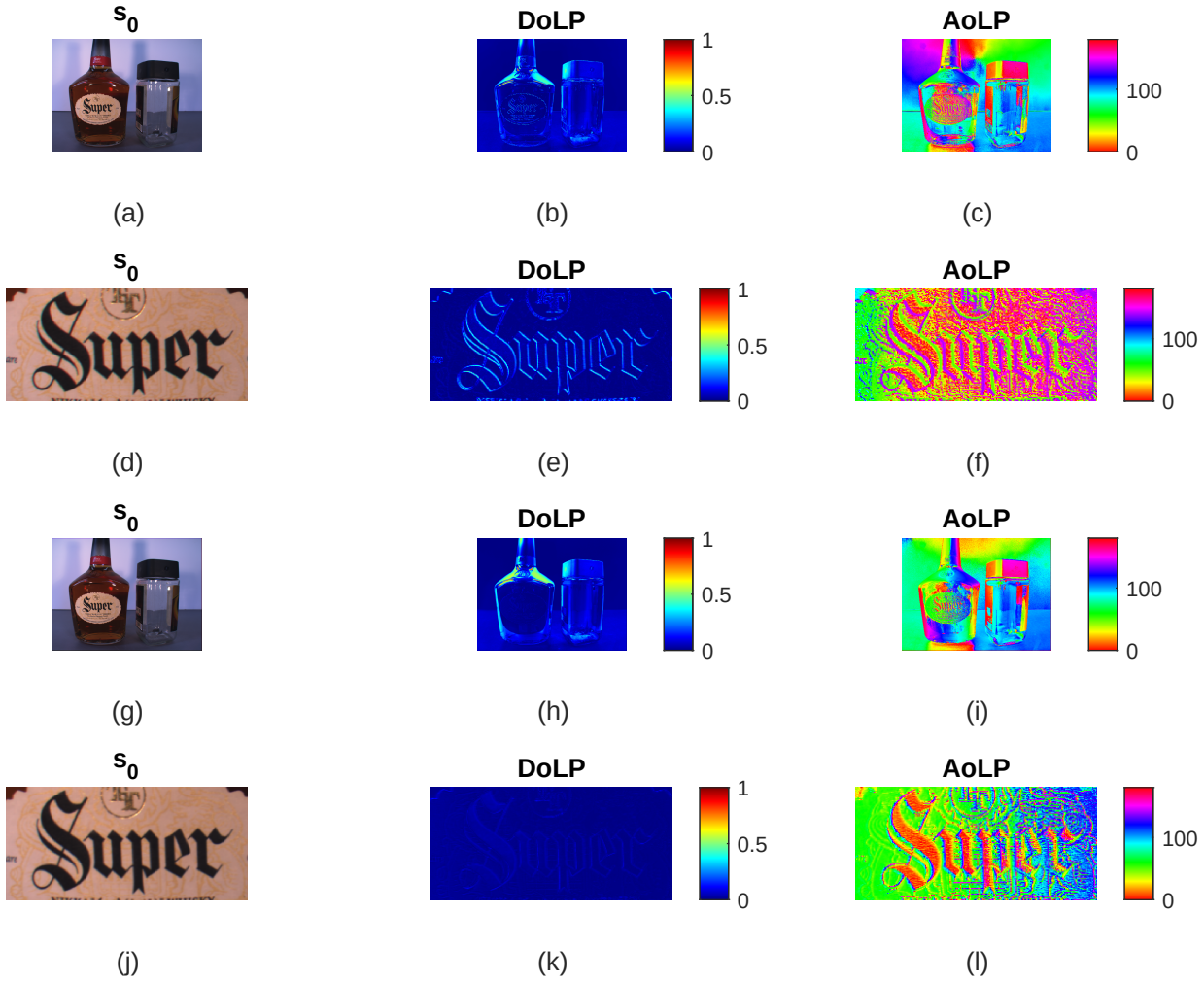

Figure 1: scene 'bottle' from Morimatsu *et al.*'s dataset.[7] (a,d,g,j) are classic RGB displays, (b,e,h,k) correspond to *DoLP* in the green band and (c,f,i,l) to *AoLP* in the green band. (d)-(f) are close-ups of (a)-(c) and (j-l) are close-ups of (h)-(i).(a)-(f) images correspond to raw data from Morimatsu *et al.*'s database, (g)-(k) correspond to registered data.

Table 4: Shifts (in pixels) between polarization directions (0°, 45°, 90° and 135°): average and maximum figures for all datasets (green band).

dataset	**Forknet**[3]	**Wen2019**[5]	**Morimatsu**[7]	**Wen2021a**[10]
Average shift	1.13	0.10	0.34	0.24
Maximum shift	1.90	0.16	0.62	0.43

5. PREPARING HD POLARIZATION IMAGES

5.1 Setup description

Considering the lack of very high definition high bit-depth polarimetric images, we decided to capture sharp high resolution (20 Mp) 12-bit monochrome polarization images. We used a CMOS Lucid Vision camera TRI200S equipped either with an Edmund Optics 25mm f/1.8 objective lens or with a Fujinon 16mm f/1.8 objective lens. Finding an objective lens that can work in conjunction with this sensor is not obvious since the sensor has a 1" diagonal and a 2.4 µm pitch. We used a rotating polarizer in front of the objective lens and captured data in the 4 classic directions 0°, 45°, 90° and 135°. Provided incident illumination is not polarized.

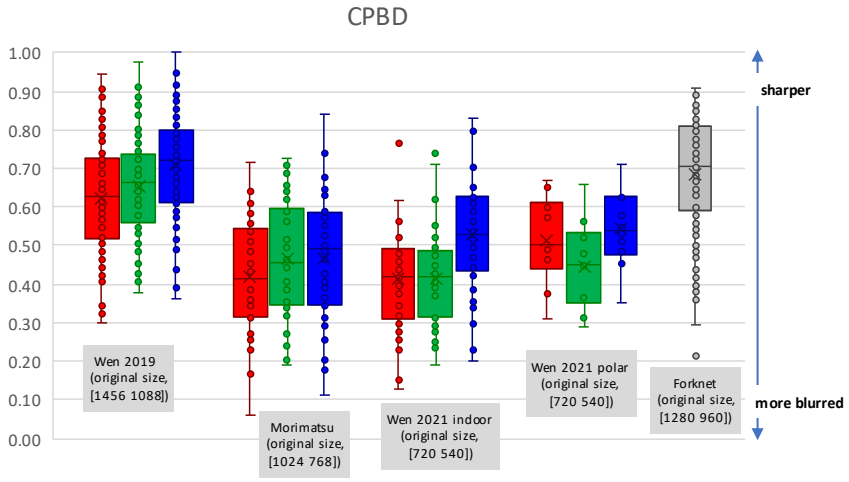

Figure 2: CPBD figures for non-mosaiced datasets reported as interval plots. Color bands are considered separately. The sharper the images, the higher the CPBD.

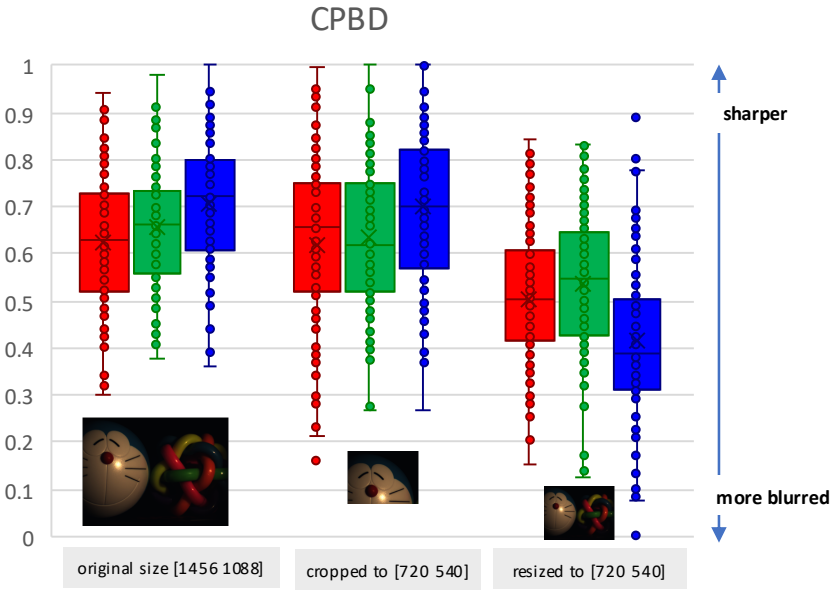

Figure 3: CPBD figures for Wen *et al.*'s 2019 dataset reported as interval plots. Figures are provided for images in their original size (1456x1088), for cropped images (720x540) and for images resized to 720x540.

Images are captured in the maximum available definition (20 Mp), in 12-bit mode at the camera maximum frame rate which is only 3.5 fps with the Gigabit internet interface. Since we average 50 images to lower noise, the acquisition time for each polarization direction is 14.3 s. Therefore, it seems difficult at this point to organize outdoor acquisitions with this configuration.

We used as a preliminary target reference patterns spread on a 7x5 grid printed on a A4 paper sheet. Both lenses produced a noticeable distortion. Fig. 5 depicts the reference pattern acquired at 495 mm from the camera with the 16mm lens opened at f/11 and reports the produced distortion. The reference marks are the white '+'s. Since the target is not centered (the image is actually cropped), it is difficult to model a distortion, but it seems we have a barrel distortion.

5.2 Reference target polarimetric acquisitions

As expected, rotating the polarizer creates a shift which is easily visible when displaying s_1, *DoLP* or *AoLP*. Fig. 6 displays close-ups of the bottom-left '+' of Fig. 5(a). Let us look at the left column, which describes

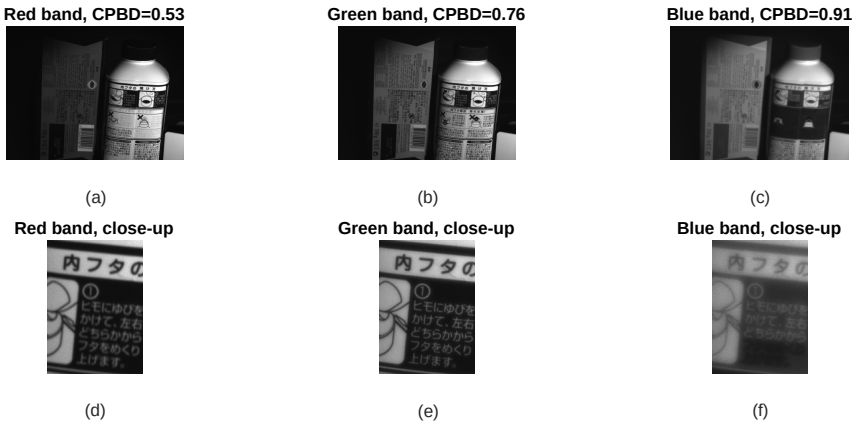

Figure 4: scene #44 from Wen *et al.*'s 2019 dataset. R, G and B bands are displayed for I_0 image. CPBD figures appear not to fit the reader's perception of blur.

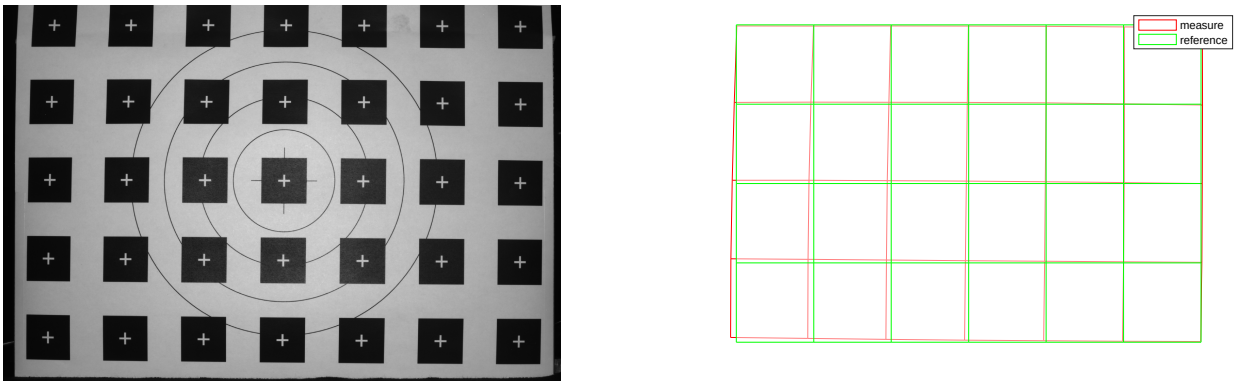

Figure 5: (a): reference target captured with 16mm lens at f/11, I_0 image. (b): grid estimated from '+' positions in (a)

results obtained when computing the polarization metrics from (1) and (2). Unexpected edges appear on s_1, as well as on $DoLP$. This shift is estimated and corrected using Guizar-Sicairos *et al.*'s technique[25] which operates a rigid subpixel translation. Results are reported in the center column of Fig. 6. Registration of I_{45}, I_{90} and I_{135} onto I_0 provides minor improvement: edges are still very visible on $DoLP$. If we look at other patches in the entire $DoLP$ image (not reported here), we see that registration sometimes worked better: in some parts of the image, artifact edges almost completely disappeared. Finally, we decided to evaluate the shifts locally for the 7x5 elementary patches with the images already registered by Guizar-Sicairos *et al.*'s technique. They are reported in Tab. 5 (left part).

Table 5: Residual shifts (in pixels) along the 7x5 grid in the reference pattern described in Fig. 5a after registration with Guizar-Sicairos *et al.*'s algorithm (left) and with our adaptive registration algorithm (right). These figures correspond to the maximum shift between I_0, I_{45}, I_{90} and I_{135}.

2.24	1.87	1.70	1.54	1.88	2.34	2.64
1.91	1.89	1.82	1.80	2.12	2.39	2.48
1.97	2.00	2.13	2.22	2.41	2.56	2.44
1.90	2.07	2.28	2.59	2.83	2.95	2.62
1.62	2.13	2.25	2.85	3.31	3.45	2.80

0.04	0.07	0.06	0.04	0.04	0.07	0.05
0.01	0.02	0.05	0.02	0.02	0.00	0.04
0.05	0.05	0.01	0.05	0.04	0.01	0.03
0.10	0.07	0.10	0.03	0.04	0.02	0.01
0.14	0.01	0.09	0.04	0.03	0.05	0.03

For each patch, we reported the maximum shift between any of the images I_0, I_{45}, I_{90} and I_{135}. We can see

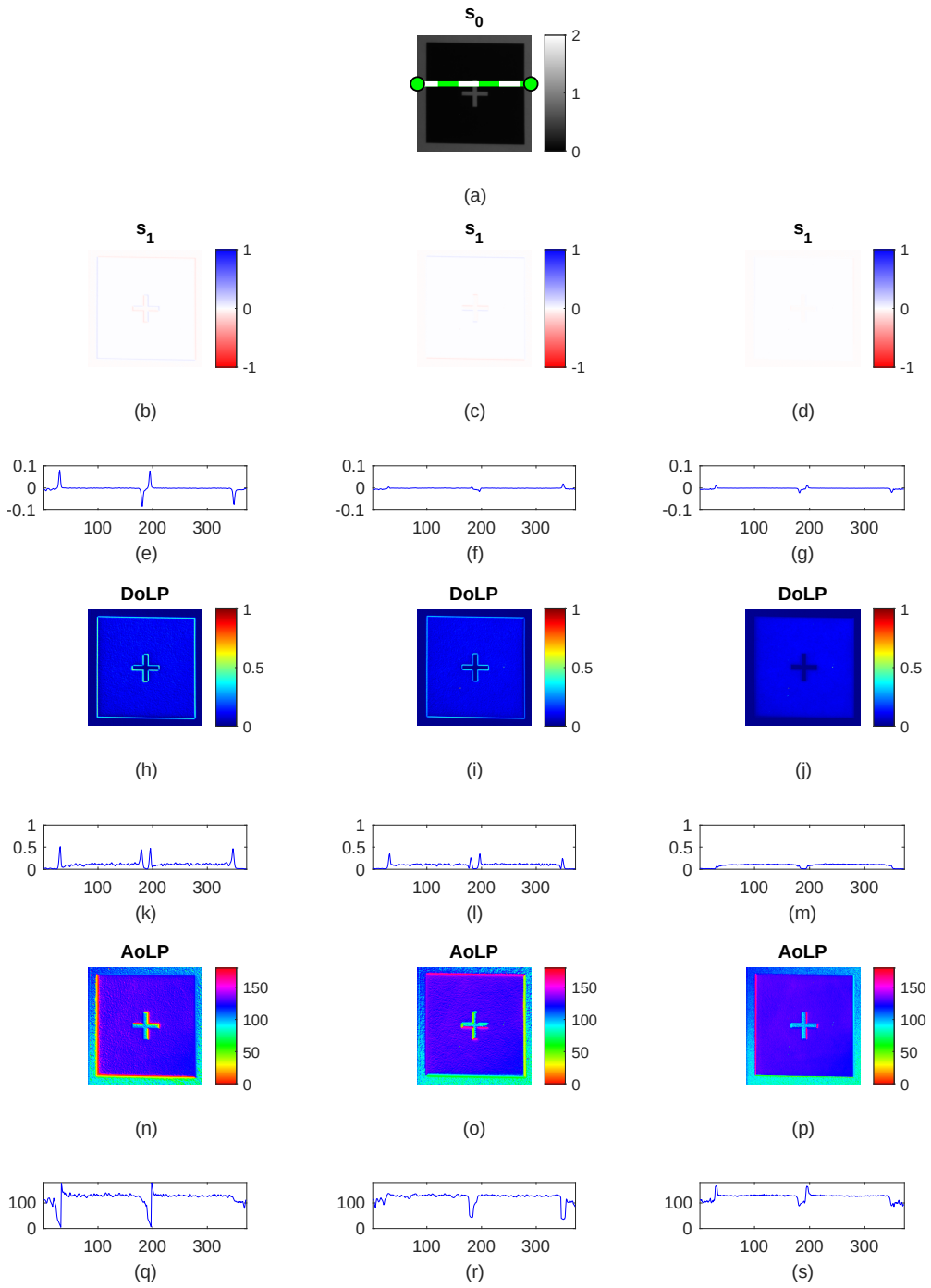

Figure 6: close-ups of the bottom left patch of the reference target. (a) shows s_0 the intensity image. Subimages in the left column depict results without prior registration of the raw images I_0, I_{45}, I_{90} and I_{135}. Subimages in the center column depict results with registration of the raw images I_{45}, I_{90} and I_{135} onto I_0 according to Guizar-Sicairos *et al.*[25] Subimages in the right column depict results with our adaptive registration of the raw images I_{45}, I_{90} and I_{135} onto I_0. The third, fifth and seventh rows ((e)-(g), (k)-(m), (q)-(s)) respectively report profiles of the images of the second, fourth and sixth rows ((b)-(d), (h)-(j), (n)-(p)) along the location described by dashed green segment in subfigure (a).

that these shifts, sometimes nearly as high as 3 pixels, are therefore likely to create huge polarimetric artifacts.

We tried several techniques to register the images, taking into account rotation and scale as well as translation, but none of these classic techniques brought a significant improvement. Alternatively, we decided to implement a warping algorithm to register the images. For each of the polarization images I_{45}, I_{90} and I_{135}, the shifts with I_0 are evaluated at the center of each of the 7x5 patches with Guizar-Sicairos *et al.*'s technique. Then a 2-D fourth degree polynomial deformation function is determined for each I_{45}, I_{90} and I_{135} at the 7x5 grid points and used to warp them onto I_0. The maximum shifts are locally evaluated and reported in Tab. 5 (right part). With our adaptive registration, the shifts are considerably lower than those obtained with Guizar-Sicairos *et al.*'s rigid registration. Fig. 7 shows the example of the '+' of the bottom left patch. We display simultaneously I_0 and I_{90} with the help of color: colors appear in the case of shift between the two images. Without registration, a large shift is visible. With classic registration, the shift is lower, but still significant, with artifact edges larger than 5 pixels. With the improved adaptive registration we propose, the shift is hardly visible, the image presents almost no color. The images corresponding to our adaptive registration are displayed in the right column of Fig.

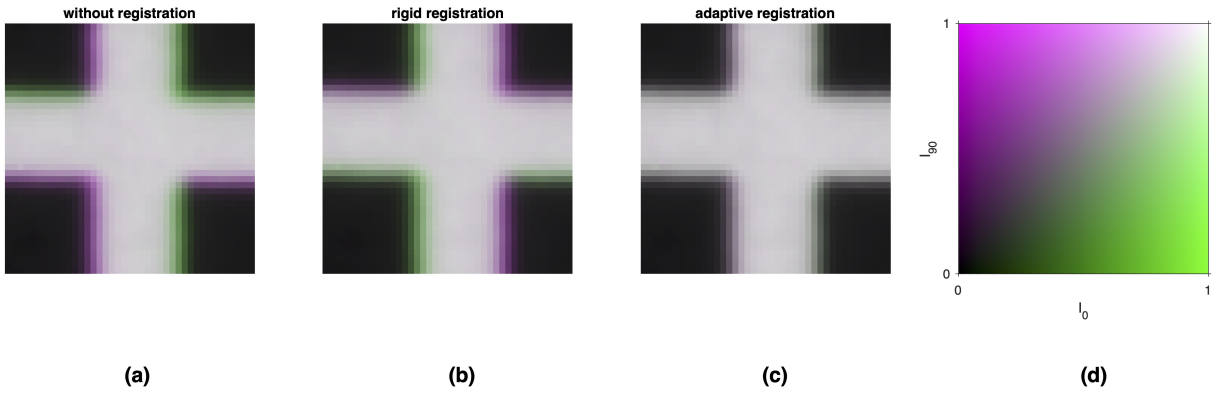

Figure 7: close-up of the bottom left patch of the reference target depicted Fig. 5a when we display I_0 and I_{90} at the same time. The sub-images are 80 pixel wide. (a): without registration, (b): with Guizar-Sicairos *et al.*'s registration, (c): with our adaptive registration. (d) depicts the colorbar we used.

6.

Considering $DoLP$, with the adaptive registration, artifacts edges completely disappeared: there was probably no polarization information on edges. On the profile plot (j), $DoLP$ appears smoother than on profiles (k) or (l): registration considerably lowered noise. Considering $AoLP$, improved registration also acted as a denoiser, but edge information is still visible; we cannot assess whether it be artifacts or not. The computational cost of all these processings is moderate, much smaller than the time required acquiring the images. It is reported in Tab. 6. Guizar-Sicairos *et al.*'s technique proves faster, at the expense of poorer registration quality.

Table 6: Computation times for the various registration algorithms (per polarization direction) on an Apple MacBook with M2 Max under Matlab R2022b.

algorithm	Shift/deformation estimation	Registration
Guizar-Sicairos *et al.*	1.70 s	0.10 s
Ours	3.90 s	2.64 s

5.3 Real-world scene polarimetric acquisition

The same setup, with the same configuration (focus and lens aperture), was used to acquire a real-world 3D scene, depicted in Fig. 8. Fig. 8a reports the scene capture by a smartphone, with a different viewing angle and an unknown gamma. Fig. 8b reports the scene capture by the 20 Mp camera with gamma set to 1. The scene appears much darker (saturations are avoided except in specular reflection zones), but we verified that the 12-bit acquisition preserves information in dark zones. We estimated CPBD from the 12-bit I_0 image and obtained

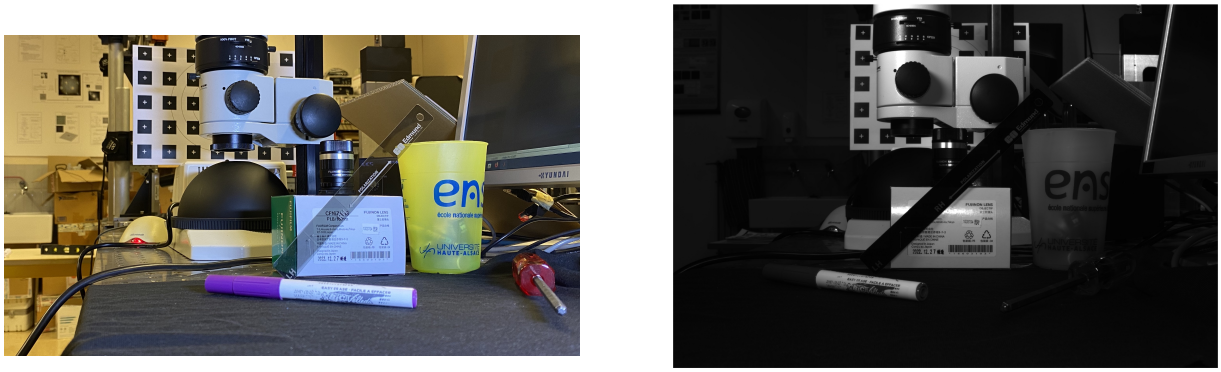

(a) (b)

Figure 8: real-world 3D scene used for experiments, shot with a smartphone under ambient light (a) or with the 20Mp camera with a polarizer under controlled illumination (b). The two images have different viewing angles and camera gamma settings.

CPBD=0.75. It corresponds to a rather sharp image. We simulated an 8-bit acquisition, it would have led to CPBD=0.32.

We evaluated polarization metrics without registration, with classic rigid registration and with our improved registration. For our algorithm, the deformation inverse model is that previously estimated with the reference target. We report results for *DoLP* (Fig. 9). The rigid registration provides significant improvement, reducing artifacts at the edges. Using our improved registration provides an extra significant improvement, visible on close-ups.

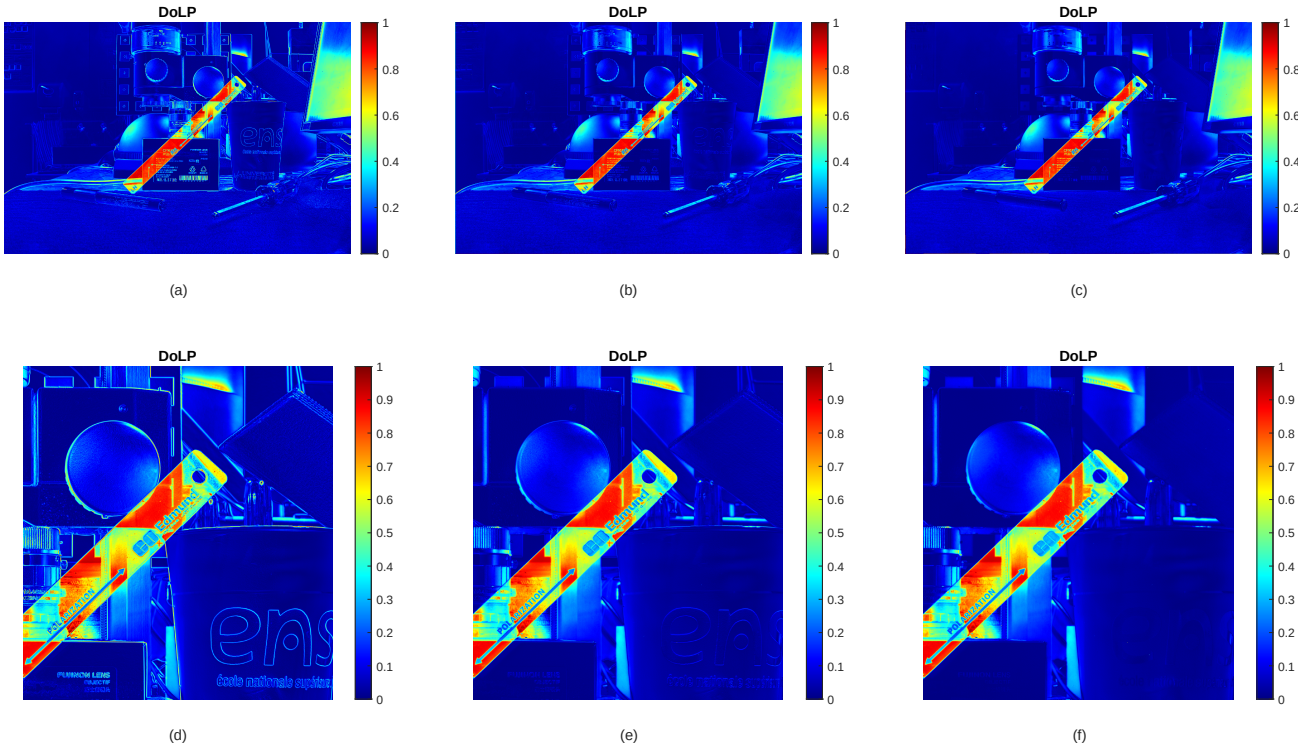

Figure 9: DoLP images for a real world scene, without registration (a), with rigid registration (b) and with our adaptive registration (c). (d)-(f) are close-ups of the previous images.

6. DISCUSSION

Identifying polarization datasets and comparing their basic characteristics is not that complicated, even if the articles reporting the making of these databases do not always give precise information. Benchmarking these various databases by assessing the quality of the images is much more complex. We only considered the quality of the individual polarization images with blur metrics, eventually their registration, but we did not take their polarimetric content into account, as Sargent *et al.*[6] did for their own dataset. The non-interpolated 4 datasets we benchmarked[3,5,7,10] proved of overall good quality, but we aimed to produce a data set with higher definition and higher bit-depth.

But producing high definition high bit-depth polarization images proves a challenging task. It requires a high quality registration of the different channels. Until now, with low definition images (let's say below 1 Mpixel), a rigid registration such as Guizar-Sicairos *et al.*'s was necessary and sufficient to avoid most polarization artifacts: this technique can estimate and fix very tiny shifts, even 1/20th pixel, which is usually admitted to be met in order to avoid most problems. But with cameras producing larger images, with larger sensors and a small pixel pitch, commercial objective lenses exhibit significant distortions resulting in artifacts larger than a pixel. This distortion can be finely characterized and with the correction technique we proposed, artifacts can be reduced within 0.15 pixels. For instance, on our reference target printed on a paper sheet, so with a low polarization configuration, it allowed us to get $DoLP$ images with reduced noise and even more reduced polarization artifacts. On the $AoLP$ images, the paper grain clearly appears, whereas it was blurred without proper registration. As far as a real world scene was considered, results were also spectacular, with major polarization artifacts cancelled. Some edge information still remains, but without any known model of the scene, it is unclear whether this is genuine polarization information or artifacts.

In this preliminary work, we only produced gray-leveled images but in the future, a color version could be implemented either by tuning the illumination (with a liquid crystal filter for instance) or by adding color filters in front of the polarization state analyser.[10] This latter solution may produce additional shifts between color bands, but the technique we implemented for the registration of polarization channel could be extended to register the color bands.

So technically there is an efficient solution to the registration problem of HD images, but with a major limitation: a proper geometric calibration with a reference target was necessary, in the exact same conditions of lens aperture, lens focus and polarizer orientation as in the final scene capture. This technique is therefore rather dedicated to laboratory experiments and may be difficult to implement in outdoor conditions for routine operations.

7. CONCLUSION

We first made a review of existing imaging polarization databases and datasets. We focused on databases made with full definition sensors (without any array of microfilters) that can be used for testing demosaicing algorithms produced by sensors equipped with arrays of color filters and/or microgrid polarizers. We showed that these databases contained raw data that must be used with much caution: for a given image, either the various polarization bands -or color bands- are not aligned or they are aligned, but present blurry content.

We decided to produce high definition polarization scenes with polarization channels properly registered and rather sharp images. We showed the registration of the various bands is not trivial, since the images suffer from significant distortion due to the optics and cannot be registered with a classic 2-D translation. We proposed an adaptive registration procedure which required a proper geometric calibration. Hence, high-definition polarization images have been produced, with extremely reduced polarization artifacts.

Existing databases have sometimes been used for the definition and evaluation of state-of-art learning-based and interpolation-based demosaicing algorithms without proper prior registration. As a future work, it would be very important to study the impact of the registration in the specific context of benchmarking demosaicing algorithms.

ACKNOWLEDGMENTS

This work was supported by the ANR JCJC SPIASI project, grant ANR-18-CE10-0005 of the French Agence Nationale de la Recherche.

The authors would like to thank all the researchers that made their datasets available and they also would like to thank Adrien Bigué (ENS Paris Saclay) for revising the English of the manuscript.

REFERENCES

[1] Abubakar, A., Zhao, X., Li, S., Takruri, M., Bastaki, E., and Bermak, A., "A block-matching and 3-d filtering algorithm for gaussian noise in dofp polarization images," *IEEE Sens. J.* **18**, 7429–7435 (2018).

[2] Lapray, P.-J., Gendre, L., Bigué, L., and Foulonneau, A., "Database of polarimetric and multispectral images in the visible and nir regions," in [*Unconventional Optical Imaging*], *Proc. SPIE* **10677**, 1067738 (2018).

[3] Zeng, X., Luo, Y., Zhao, X., and Ye, W., "An end-to-end fully-convolutional neural network for division of focal plane sensors to reconstruct s0, dolp, and aop," *Opt. Express* **27**, 8566–8577 (2019).

[4] Qiu, S., Fu, Q., Wang, C., and Heidrich, W., "Polarization demosaicking for monochrome and color polarization focal plane arrays," in [*Conference on Vision, Modeling, and Visualization*], The Eurographics Association (2019).

[5] Wen, S., Zheng, Y., Lu, F., and Zhao, Q., "Convolutional demosaicing network for joint chromatic and polarimetric imagery," *Opt. Lett.* **44**, 5646–5649 (2019).

[6] Sargent, G. C., Ratliff, B. M., and Asari, V. K., "Conditional generative adversarial network demosaicing strategy for division of focal plane polarimeters," *Opt. Express* **28**, 38419–38443 (2020).

[7] Morimatsu, M., Monno, Y., Tanaka, M., and Okutomi, M., "Monochrome and color polarization demosaicking using edge-aware residual interpolation," in [*2020 IEEE International Conf. on Image Processing (ICIP)*], 2571–2575, IEEE (2020).

[8] Morimatsu, M., Monno, Y., Tanaka, M., and Okutomi, M., "Monochrome and color polarization demosaicking based on intensity-guided residual interpolation," *IEEE Sens. J.* **21**, 26985–26996 (2021).

[9] Ba, Y., Gilbert, A., Wang, F., Yang, J., Chen, R., Wang, Y., Yan, L., Shi, B., and Kadambi, A., "Deep shape from polarization," in [*ECCV 2020*], *LNCS* **12369**, 554–571, Springer International Publishing, Cham (2020).

[10] Wen, S., Zheng, Y., and Lu, F., "A sparse representation based joint demosaicing method for single-chip polarized color sensor," *IEEE Trans. Image Proc.* **30**, 4171–4182 (2021).

[11] Wen, S., Zheng, Y., and Lu, F., "Polarization guided specular reflection separation," *IEEE Trans. Image Proc.* **30**, 7280–7291 (2021).

[12] Blin, R., Ainouz, S., Canu, S., and Meriaudeau, F., "Multimodal polarimetric and color fusion for road scene analysis in adverse weather conditions," in [*2021 IEEE International Conf. on Image Processing (ICIP)*], 3338–3342, IEEE (2021).

[13] Sun, Y., Zhang, J., and Liang, R., "Color polarization demosaicking by a convolutional neural network," *Opt. Lett.* **46**, 4338–4341 (2021).

[14] Sattar, S., Lapray, P.-J., Aksas, L., Foulonneau, A., and Bigué, L., "Snapshot spectropolarimetric imaging using a pair of filter array cameras," *Opt. Eng.* **61**, 043104 (2022).

[15] Lei, C., Qi, C., Xie, J., Fan, N., Koltun, V., and Chen, Q., "Shape from polarization for complex scenes in the wild," in [*2022 IEEE/CVF Conf. on Computer Vision and Pattern Recognition (CVPR)*], 12622–12631, IEEE (2022).

[16] Ono, T., Kondo, Y., Sun, L., Kurita, T., and Moriuchi, Y., "Degree-of-linear-polarization-based color constancy," in [*2022 IEEE/CVF Conference on Computer Vision and Pattern Recognition (CVPR)*], 19708–19717, IEEE (2022).

[17] Kurita, T., Kondo, Y., Sun, L., and Moriuchi, Y., "Simultaneous acquisition of high quality rgb image and polarization information using a sparse polarization sensor," in [*2023 IEEE/CVF Winter Conf. on Applications of Computer Vision (WACV)*], 178–188, IEEE (2023).

[18] Liu, J., Duan, J., Hao, Y., Chen, G., Zhang, H., and Zheng, Y., "Polarization image demosaicing and rgb image enhancement for a color polarization sparse focal plane array," *Opt. Express* **31**, 23475–23490 (2023).
[19] Goldstein, D., [*Polarized light*], Marcel Dekker, New-York Basel (2003 (second edition)).
[20] Wolff, L. B., Mancini, T. A., Pouliquen, P., and Andreou, A. G., "Liquid crystal polarization camera," *IEEE Trans. Robot. Autom.* **13**, 195–203 (1997).
[21] "Polarization image sensor technology polarsens™ | image sensor for industrial use." Sony Semiconductors, https://www.sony-semicon.com/en/technology/industry/polarsens.html (Accessed: 28 July 2023).
[22] Mihoubi, S., Lapray, P.-J., and Bigué, L., "Survey of demosaicking methods for polarization filter array images," *Sensors* **18**, 3688 (2018).
[23] Bigué, L., "Polarization imaging datasets." GitHub (13 July 2023), https://github.com/laurent-bigue/Polarization-imaging-datasets (Accessed: 28 July 2023).
[24] Smith, M., Woodruff, J., and Howe, J., "Beam wander considerations in imaging polarimetry," in [*SPIE's International Symposium on Optical Science, Engineering, and Instrumentation*], *Proc. SPIE* **3754** (1999).
[25] Guizar-Sicairos, M., Thurman, S. T., and Fienup, J. R., "Efficient subpixel image registration algorithms," *Opt. Lett.* **33**, 156–158 (2008).
[26] Pertuz, S., Puig, D., and Garcia, M. A., "Analysis of focus measure operators for shape-from-focus," *Pattern Recognit.* **46**, 1415–1432 (2013).
[27] Crété, F., Dolmière, T., Ladret, P., and Nicolas, M., "The blur effect: perception and estimation with a new no-reference perceptual blur metric," in [*Human, Vision and Electronic Imaging XII*], *Proc. SPIE* **6492** (2007).
[28] Narvekar, N. and Karam, L., "A no-reference image blur metric based on the cumulative probability of blur detection (cpbd)," *IEEE Trans. Image Proc.* **20**, 2678–2683 (2011).